Power scaling of normal-dispersion continuum generation using higher-order modes in microstructured optical fibers

To be published in Optics Letters:

Title: Power scaling of normal-dispersion continuum generation using higher-order modes in microstructured optical fibers

Authors: Federica Poli,Jesper Laegsgaard

Accepted: 13 December 21

Posted 13 December 21

DOI: https://doi.org/10.1364/OL.448523

Power scaling of normal-dispersion continuum generation using higher-order modes in microstructured optical fibers

FEDERICA POLI[1] AND JESPER LÆGSGAARD[2,*]

[1] Department of Engineering and Architecture, University of Parma, I-43124 Parma, Italy
[2] DTU Fotonik, Department of Photonics Engineering, Technical University of Denmark, DK-2800 Kongens Lyngby, Denmark
[*] Corresponding author: jlag@fotonik.dtu.dk

Compiled December 10, 2021

The use of a higher-order HE_{12}-like mode to produce weak normal dispersion over a substantial wavelength range in a microstructured optical fiber is investigated numerically. It is shown that the effective area, and thereby the pulse energy, can in this way be scaled by an order of magnitude compared to using the fundamental mode in a single mode fiber. Multimode nonlinear simulations indicate that nonlinear mode coupling will not disturb single-mode operation in the HE_{12} mode at least up to the threshold where polarization modulational instability sets in.

OCIS codes: (060.4005) Microstructured fibers; (060.4370) Nonlinear optics, fibers;(060.7140) Ultrafast processes in fibers.

http://dx.doi.org/10.1364/ao.XX.XXXXXX

Supercontinuum generation (SCG) from femtosecond (fs) pump pulses by self-phase modulation and wave breaking in fibers with weak all-normal dispersion (commonly denoted ANDi fibers) has in recent years become an object of intense research [1–3]. The deterministic nature of the nonlinear processes results in low noise and excellent shot-to-shot coherence up to a power threshold set by the appearance of Raman and possibly polarization modulational instability [4, 5]. Compared to picosecond-pumped SCG in fibers with anomalous dispersion at the pump wavelength [6], this is a distinct advantage, since the latter approach relies on pulse breakup by modulational instabilities seeded by quantum noise, resulting in chaotic shot-to-shot variations of spectra and pulse profiles [7], and a high degree of complexity in both spectral and temporal domains. Disadvantages of ANDi-SCG are the need for fs pump pulses, somewhat narrower spectra (although bandwidths of several hundred nm are routinely generated), and severe limitations in power scaling. The present theoretical study aims to resolve the latter issue through SCG in higher-order modes (HOMs).

The key technological enabler for ANDi-SCG was the realization that flat dispersion profiles with a small negative value of the dispersion coefficient D could be obtained in microstructured optical fibers with relatively small airholes, and very small core diameters on the order of 2.5 μm for operation in the Yb gain band just above 1 μm [1]. The need for a small core size obviously impedes power scaling, and typical pump pulse energies are in the few-nJ or even sub-nJ range. A similar limitation is encountered when designing for anomalous dispersion around 1 μm, although the core diameters are in this case typically around 3-5 μm. It is by now well appreciated that the use of HOMs can enable anomalous modal dispersion at wavelengths where the material dispersion is normal, even in very large cores, thus providing a route to power scaling of anomalous-dispersion SCG and related processes such as dispersive-wave generation or four-wave mixing [8–12]. A pertinent question is then whether a similar potential exists for engineering of large-core ANDi fibers.

The conventional ANDi design consists of a single-mode microstructured fiber with a triangular array of airholes, where the solid single-mode core is defined by a single missing airhole, here denoted a 1C design [1]. We have found that similar dispersion properties to those of the 1C HE_{11}-like mode can be achieved in the HE_{12}-like mode of an enlarged core defined by seven missing airholes, which we will denote a 7C-design.

In Fig. 1 the dispersion coefficient (D, top panel), confinement loss (CL, middle panel) and effective area (A_{eff}, bottom panel) are shown for the 1C HE_{11} mode and the 7C HE_{12} modes. These parameters, as well as the mode field distributions, have been evaluated with a full-vector modal solver based on the finite-element method [13, 14], taking into account the Sellmeier equation to calculate the silica refractive index [15]. All designs are characterized by the center-to-center distance between neighbouring airholes, Λ, and the ratio d/Λ where d is the airhole diameter. The fibers have been designed to have similar dispersion around 1 μm, but the HE_{12} mode in the 7C design with d/Λ=0.35 has a steeper curvature, especially towards longer wavelengths. In addition, this mode deconfines completely at 1.4 μm and already shows dB/cm loss around 1.25 μm. Since the 1C design allows continuum generation out to wavelengths around 1.5 μm (see below), this is a significant drawback of the HOM approach.

The situation may be remedied by enlarging the outer airholes in the 7C design to improve confinement, while retaining d/Λ=0.35 for the holes closest to the core to control dispersion. A similar approach was earlier demonstrated to be experimen-

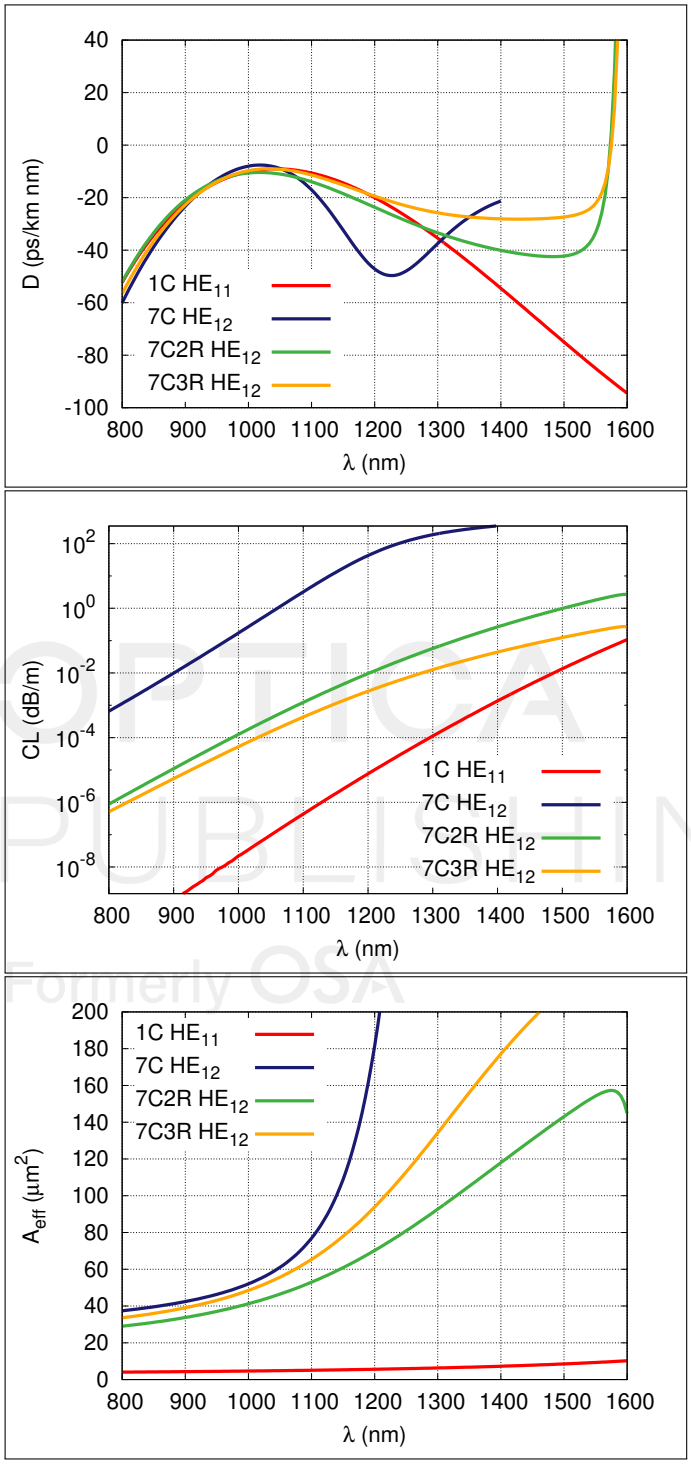

Fig. 1. Dispersion coefficient D (top), confinement loss CL (middle) and effective area A_{eff} (bottom) for the 1C, 7C, 7C2R and 7C3R designs, with Λ=1.5 μm, 2.5 μm, 2.1 μm and 2.3 μm respectively.

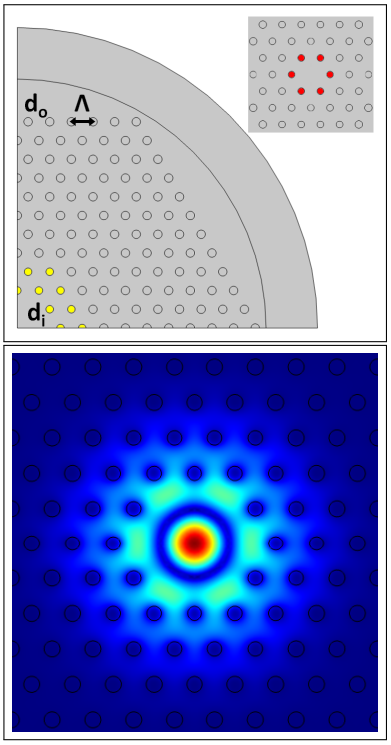

Fig. 2. Top: Schematic depiction of the 7C2R structure with inner hole diameter d_i (yellow holes), outer hole diameter d_o and pitch Λ. Inset shows 1C core, the red holes are removed to form the 7C core. Bottom: Electric-field modulus at 1 μm for the HE_{12} mode at 1 μm in the 7C2R structure.

tally feasible in 1C fibers [16]. In the designs denoted 7C2R and 7C3R the airholes in the two or three innermost 'rings' around the core, respectively, have been kept at d_i/Λ=0.35, whereas the outer airholes are enlarged to d_o/Λ=0.39. A schematic depiction of the 7C2R design is shown in the top panel of Fig. 2. The result is a dramatic improvement of CL, making the HE_{12} mode useful up to at least 1.6 μm. In addition, the dispersion curve is flattened and comparable to the 1C HE_{11} dispersion at intermediate wavelengths, and even flatter beyond 1.3 μm. The HE_{12} mode in these designs is confined to the core for wavelengths around 1μm and shorter, then gradually expands into the 'inner cladding' with d/Λ=0.35, leading to an increased slope of the A_{eff} curve, without deconfinement setting in. The electric-field modulus of the HE_{12} mode in the 7C2R design at a wavelength of 1 μm is shown in the bottom panel of Fig. 2. The A_{eff}-curves in Fig. 1 show the 7C3R area expanding faster than in the 7C2R structure due to the larger area of the inner cladding.

The HE_{12} A_{eff} at 1.064 μm is 48 μm^2 in the 7C2R design, and 58 μm^2 in the 7C3R fiber, whereas the HE_{11} A_{eff} in the 1C design is 4.9 μm^2. Given the similar dispersion properties and a negligible CL for propagation lengths of $\sim$ 10 cm, these results suggest that an order-of-magnitude scaling of pulse energy for a given nonlinear process should be within reach of the HOM approach.

Nonlinear simulations are performed by two approaches: A conventional two-mode approach, considering two polarization states of the same (HE_{12}-like) eigenmode using the effective-area approximation [17, 18] is used to quickly explore the power levels needed to obtain efficient SCG within the limits set by

polarization modulational instability [19]. In addition, multi-mode (MM) simulations incorporating all 14 guided modes are carried out for the 7C2R design using a recently developed real-space gaussian quadrature approach to evaluate the nonlinear operator [20, 21]. The simulation results shown below were all obtained with linearly polarized gaussian-shaped input pulses having 50 fs full width at half maximum, and propagating in 10 cm of fiber. To study the impact of polarization modulational instability and possibly other intermodal couplings, quantum noise in the form of one random-phase photon per frequency mode was added to the input pulse.

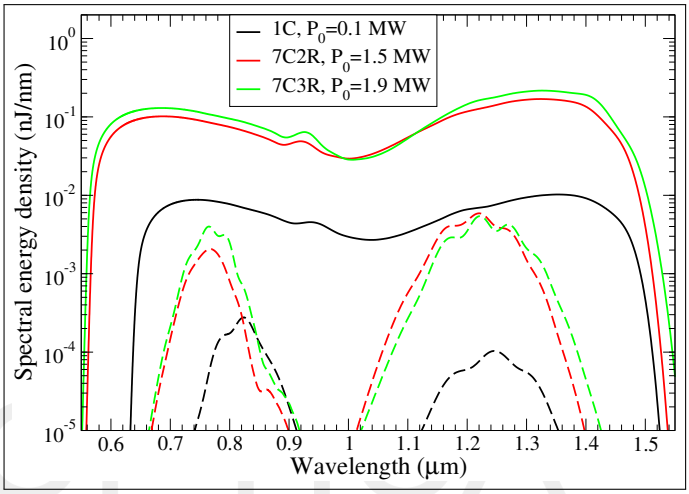

Fig. 3. Output spectra after 10 cm propagation in 1C, 7C and 7C2R fibers for a 50 fs pump pulse at 1.064 μm with peak power P_0. Solid lines represent the input polarization, whereas dashed lines represent the orthogonal (quantum-noise-seeded) polarization. Only the two HE_{12} polarization states are included in the simulation.

In Fig. 3 two-mode output spectra for the 1C, 7C2R and 7C3R designs are shown. For a fair comparison, the peak power P_0 of the input pulse was adjusted to just below the level where 1% of the output power appeared in the orthogonal polarization. For the 1C design, this limit was reached around P_0=100 kW, whereas for the 7C2R and 7C3R designs pumped in the HE_{12} mode, P_0 levels of 1.5 and 1.9 MW, respectively, were reached. Thus, the use of the HE_{12} mode enables a power scaling of more than an order of magnitude, corresponding to the effective-area scaling. The intensity and fluence level are therefore similar to those obtained in single-mode ANDi fibers [2], and well within the ~1-2 J/cm^2 fluence limit for sub-100 fs pulses which can be estimated from studies of dielectric breakdown in silica [22]. It is also interesting to note that the 7C designs provide a broader continuum for comparable levels of cross-polarization coupling. The P_0 difference of ~ 25% between 7C2R and 7C3R is roughly consistent with the difference in A_{eff} at the pump wavelength. The notable differences in A_{eff} and dispersion properties on the long-wavelength side of the pump appear to have little impact on the power scaling and spectral shape.

The output spectrum for full MM propagation with P_0=1.5 MW in the 7C2R structure, averaged over 30 different quantum-noise seeded simulations [7], is shown in Fig. 4. The spectrum in the HE_{12x} (pump) mode compares well with the two-mode simulation. Also the HE_{12y} spectra compare reasonably well, and the coupling to the orthogonal polarization state of the HE_{12}

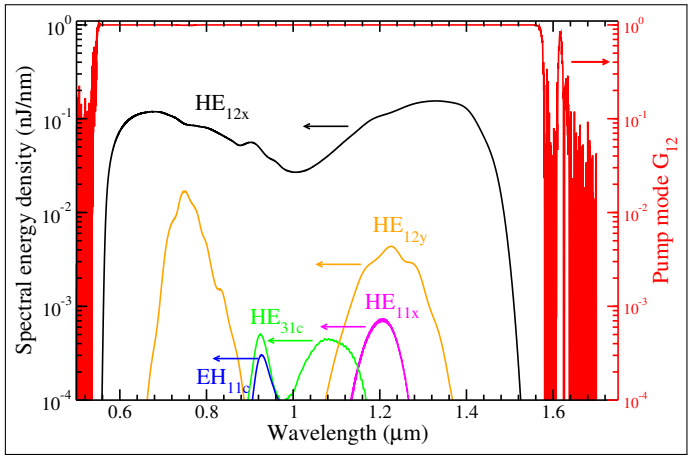

Fig. 4. Output spectrum and coherence function of a full MM simulation with P_0=1.5 MW in the 7C2R structure.

mode is seen to be dominant. Three other modes have noticeable populations, with all other mode types being below 10^{-5} nJ/nm over the entire spectral range. The HE_{11x} mode has the same azimuthal symmetry and polarization as the pump mode, but the two modes are widely separated in effective index. The other higher-order modes have mixed polarizations, but can be distinguished according to the E_z field component having either $\cos(m\phi)$ (c) or $\sin(m\phi)$ (s) azimuthal dependence. The HE_{31c} and EH_{11c} modes share this angular dependence with the pump mode, and are also close in effective index. The nature of the mode couplings differ in that the HE_{12x}-HE_{12y} coupling is a continuous parametric process, and so the output HE_{12y} energy fraction grows with fiber length. Conversely, the coupling to HE_{11x}, EH_{11c} and HE_{31c} happens over the first cm of propagation, in a seemingly deterministic process. To quantify the noise properties, the frequency-resolved coherence function $G_{12}^{(m)}(\omega)$ for mode m is defined as

$$G_{12}^{(m)}(\omega) = \frac{1}{n(n-1)} \sum_{kl} \frac{A_m^{(k)*}(\omega) A_m^{(l)}(\omega)}{\mid A_m^{(k)}(\omega) A_m^{(l)}(\omega) \mid} \qquad (1)$$

where n is the number of simulations in the ensemble, and $A_m^{(k)}(\omega)$ is the field amplitude for mode m in simulation k. The red curve in Fig. 4 shows G_{12} for the pump mode. A value of 1 indicates perfect coherence. In the region where the spectrum has significant weight G_{12} is seen to be very close to 1, with only a small dip to ~0.987 occurring in the frequency band where the HE_{12y} spectrum peaks. As expected, this indicates that the upper boundary of low-noise operation with respect to input power has been identified.

Another important issue is whether the presence of other modes than the pump mode affects the femto- and picosecond contrast of compressed pulses. To investigate this in a simple way, we calculated transform-limited (flat phase) pulse profiles in all modes. This is a conservative assessment since in reality one would optimize compression of the pump mode only. The trailing half of the (symmetric) compressed pulse is shown in Fig. 5. The largest satellite peak is in the pump mode and ~10% of the main peak, whereas all other modes are suppressed by a factor 10^{-3}-10^{-4} or higher. This is then the upper bound on temporal contrast degradation due to the presence of other modes, even if the other mode orders shift temporally relative to the HE_{12x} mode. In the case of perfect alignment, the HE_{12y}

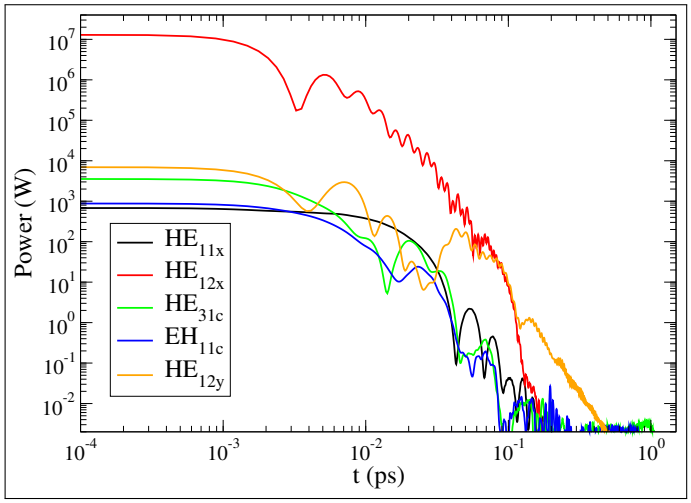

Fig. 5. Double-log plot of dechirped output pulses from the spectra in Fig. 4. Only half of the symmetric pulse profile is shown.

mode begins to dominate beyond ∼100 fs, at a suppression level of $\sim 10^{-5}$, whereas the EH_{11c} and HE_{31c} modes only become dominant beyond ∼500 fs at a suppression level of 10^{-10}.

Our nonlinear simulations do not take mode conversions from linear scattering into account. However, the smallest effective-index difference between the HE_{12} and other mode groups is $>5{\cdot}10^{-4}$ over the whole HE_{12x} 30-dB bandwidth in Fig. 4. Microdeformations coupling modes with an effective-index separation Δn_{eff} at a wavelength λ should have a spatial period corresponding to the beat length $\frac{\lambda}{\Delta n_{eff}}$. The impact of short-period fluctuations on the waveguide core is limited by the fiber outer diameter, D, and the stiffness of fiber and coating. For typical fiber coatings, one can estimate that only modes having $\Delta n_{eff} \lesssim \frac{0.1\lambda}{D}$ are susceptible to coupling [23]. This implies that an outer diameter of 2-300 μm should suffice to inhibit intermodal scattering in the fiber structure considered here. Other authors have suggested an even lower critical value of $\Delta n_{eff} < 1.5 \cdot 10^{-4}$ for HOM stability in step-index fibers [24]. In addition, the short fiber lengths required for supercontinuum generation further reduces the impact of linear mode couplings. By a similar reasoning, we do not expect significant issues with macrobending losses, and in any event it is not a practical problem to keep a 10-cm piece of fiber straight if necessary [25].

The HOM approach to power scaling is in principle open-ended, as HOMs of higher order may be leveraged to engineer dispersion in still larger cores. Ultimately, this scaling will be limited by linear and/or nonlinear mode couplings due to decreasing effective-index differences between different mode groups. In addition, it needs to be determined from simulations whether a useful curvature and bandwidth of the dispersion curve can also be achieved for higher mode orders.

In conclusion, we have presented a class of multimode microstructured fiber designs for fs-pumped coherent supercontinuum generation in the HE_{12} mode. Linear and nonlinear simulations demonstrate that an order-of-magnitude power scaling compared to single-mode designs can be achieved without detrimental effects of nonlinear mode coupling.

Disclosures. The author declares no conflicts of interest.

REFERENCES

1. A. M. Heidt, J. Opt. Soc. Am. B **27**, 550 (2010).
2. A. M. Heidt, A. Hartung, G. W. Bosman, P. Krok, E. G. Rohwer, H. Schwoerer, and H. Bartelt, Opt. Express **19**, 3775 (2011).
3. A. Rampur, D. M. Spangenberg, B. Sierro, P. Hänzi, M. Klimczak, and A. M. Heidt, Appl. Phys. Lett. **118**, 240504 (2021).
4. A. M. Heidt, J. S. Feehan, J. H. V. Price, and T. Feurer, J. Opt. Soc. Am. B **34**, 764 (2017).
5. E. Genier, P. Bowen, T. Sylvestre, J. M. Dudley, P. Moselund, and O. Bang, J. Opt. Soc. Am. B **36**, A161 (2019).
6. J. K. Ranka, R. S. Windeler, and A. J. Stentz, Opt. Lett. **25**, 25 (2000).
7. J. M. Dudley, G. Genty, and S. Coen, Rev. Mod. Phys. **78**, 1135 (2006).
8. S. Ramachandran, S. Ghalmi, J. W. Nicholson, M. F. Yan, P. Wisk, E. Monberg, and F. V. Dimarcello, Opt. Lett. **31**, 2532 (2006).
9. N. Karasawa and K. Tada, Opt. Express **18**, 5338 (2010).
10. P. Steinvurzel, J. Demas, B. Tai, Y. Chen, L. Yan, and S. Ramachandran, Opt. Lett. **39**, 743 (2014).
11. D. Jain, C. Markos, T. M. Benson, A. B. Seddon, and O. Bang, Sci. Reports **9**, 8536 (2019).
12. G. Prabhakar, P. Gregg, L. Rishoj, P. Kristensen, and S. Ramachandran, Opt. Express **27**, 11547 (2019).
13. "Comsol Multiphysics® v. 5.6," www.comsol.com. COMSOL AB, Stockholm, Sweden.
14. E. Coscelli, F. Poli, J. Li, A. Cucinotta, and S. Selleri, IEEE Photonics J. **7**, 1 (2015).
15. F. Poli, A. Cucinotta, M. Fuochi, S. Selleri, and L. Vincetti, J. Opt. Soc. Am. A **20**, 1958 (2003).
16. S. D. Rao, R. D. Engelsholm, I. B. Gonzalo, B. Zhou, P. Bowen, P. M. Moselund, O. Bang, and M. Bache, Opt. Lett. **44**, 2216 (2019).
17. J. Lægsgaard, Opt. Express **15**, 16110 (2007).
18. S. R. Petersen, T. T. Alkeskjold, C. B. Olausson, and J. Lægsgaard, Opt. Express **23**, 5954 (2015).
19. I. Bravo Gonzalo, R. D. Engelsholm, M. P. Sørensen, and O. Bang, Sci. Reports **8**, 6579 (2018).
20. J. Lægsgaard, J. Opt. Soc. Am. B **36**, 2235 (2019).
21. J. Lægsgaard, Opt. Lett. **45**, 4160 (2020).
22. B. Stuart, M. Feit, S. Herman, A. Rubenchik, B. Shore, and M. Perry, Phys. Rev. B **53**, 1749 (1996).
23. M. D. Nielsen, N. A. Mortensen, and J. R. Folkenberg, Opt. Lett. **28**, 1645 (2003).
24. S. Ramachandran, J. W. Nicholson, S. Ghalmi, M. F. Yan, P. Wisk, E. Monberg, and F. V. Dimarcello, Opt. Lett. **31**, 1797 (2006).
25. V. Degiorgio, L. Tartara, R. Cherif, and M. Zghal, Eur. Conf. on Opt. Commun. Ecoc p. 5287128 (2009).

FULL REFERENCES

1. A. M. Heidt, "Pulse preserving flat-top supercontinuum generation in all-normal dispersion photonic crystal fibers," J. Opt. Soc. Am. B **27**, 550–559 (2010).
2. A. M. Heidt, A. Hartung, G. W. Bosman, P. Krok, E. G. Rohwer, H. Schwoerer, and H. Bartelt, "Coherent octave spanning near-infrared and visible supercontinuum generation in all-normal dispersion photonic crystal fibers," Opt. Express **19**, 3775–3787 (2011).
3. A. Rampur, D. M. Spangenberg, B. Sierro, P. Hänzi, M. Klimczak, and A. M. Heidt, "Perspective on the next generation of ultra-low noise fiber supercontinuum sources and their emerging applications in spectroscopy, imaging, and ultrafast photonics," Appl. Phys. Lett. **118**, 240504 (2021).
4. A. M. Heidt, J. S. Feehan, J. H. V. Price, and T. Feurer, "Limits of coherent supercontinuum generation in normal dispersion fibers," J. Opt. Soc. Am. B **34**, 764–775 (2017).
5. E. Genier, P. Bowen, T. Sylvestre, J. M. Dudley, P. Moselund, and O. Bang, "Amplitude noise and coherence degradation of femtosecond supercontinuum generation in all-normal-dispersion fibers," J. Opt. Soc. Am. B **36**, A161–A167 (2019).
6. J. K. Ranka, R. S. Windeler, and A. J. Stentz, "Visible continuum generation in air-silica microstructure optical fibers with anomalous dispersion at 800 nm," Opt. Lett. **25**, 25–27 (2000).
7. J. M. Dudley, G. Genty, and S. Coen, "Supercontinuum generation in photonic crystal fiber," Rev. Mod. Phys. **78**, 1135–1184 (2006).
8. S. Ramachandran, S. Ghalmi, J. W. Nicholson, M. F. Yan, P. Wisk, E. Monberg, and F. V. Dimarcello, "Anomalous dispersion in a solid, silica-based fiber," Opt. Lett. **31**, 2532–2534 (2006).
9. N. Karasawa and K. Tada, "The generation of dispersive waves from a photonic crystal fiber by higher-order mode excitation," Opt. Express **18**, 5338–5343 (2010).
10. P. Steinvurzel, J. Demas, B. Tai, Y. Chen, L. Yan, and S. Ramachandran, "Broadband parametric wavelength conversion at 1μm with large mode area fibers," Opt. Lett. **39**, 743–746 (2014).
11. D. Jain, C. Markos, T. M. Benson, A. B. Seddon, and O. Bang, "Exploiting dispersion of higher-order-modes using m-type fiber for application in mid-infrared supercontinuum generation," Sci. Reports **9**, 8536 (2019).
12. G. Prabhakar, P. Gregg, L. Rishoj, P. Kristensen, and S. Ramachandran, "Octave-wide supercontinuum generation of light-carrying orbital angular momentum," Opt. Express **27**, 11547–11556 (2019).
13. "Comsol Multiphysics® v. 5.6," www.comsol.com. COMSOL AB, Stockholm, Sweden.
14. E. Coscelli, F. Poli, J. Li, A. Cucinotta, and S. Selleri, "Dispersion engineering of highly nonlinear chalcogenide suspended-core fibers," IEEE Photonics J. **7**, 1–8 (2015).
15. F. Poli, A. Cucinotta, M. Fuochi, S. Selleri, and L. Vincetti, "Characterization of microstructured optical fibers for wideband dispersion compensation," J. Opt. Soc. Am. A **20**, 1958–62 (2003).
16. S. D. Rao, R. D. Engelsholm, I. B. Gonzalo, B. Zhou, P. Bowen, P. M. Moselund, O. Bang, and M. Bache, "Ultra-low-noise supercontinuum generation with a flat near-zero normal dispersion fiber," Opt. Lett. **44**, 2216–2219 (2019).
17. J. Lægsgaard, "Mode profile dispersion in the generalised nonlinear schrödinger equation," Opt. Express **15**, 16110–16123 (2007).
18. S. R. Petersen, T. T. Alkeskjold, C. B. Olausson, and J. Lægsgaard, "Intermodal and cross-polarization four-wave mixing in large-core hybrid photonic crystal fibers," Opt. Express **23**, 5954–5971 (2015).
19. I. Bravo Gonzalo, R. D. Engelsholm, M. P. Sørensen, and O. Bang, "Polarization noise places severe constraints on coherence of all-normal dispersion femtosecond supercontinuum generation," Sci. Reports **8**, 6579 (2018).
20. J. Lægsgaard, "Full-vectorial multimode nonlinear simulations on a real-space fourier-gauss grid," J. Opt. Soc. Am. B **36**, 2235–2243 (2019).
21. J. Lægsgaard, "Multimode nonlinear simulation technique having near-linear scaling with mode number in circular symmetric waveguides," Opt. Lett. **45**, 4160–4163 (2020).
22. B. Stuart, M. Feit, S. Herman, A. Rubenchik, B. Shore, and M. Perry, "Nanosecond-to-femtosecond laser-induced breakdown in dielectrics," Phys. Rev. B **53**, 1749–1761 (1996).
23. M. D. Nielsen, N. A. Mortensen, and J. R. Folkenberg, "Reduced microdeformation attenuation in large-mode-area photonic crystal fibers for visible applications," Opt. Lett. **28**, 1645–1647 (2003).
24. S. Ramachandran, J. W. Nicholson, S. Ghalmi, M. F. Yan, P. Wisk, E. Monberg, and F. V. Dimarcello, "Light propagation with ultralarge modal areas in optical fibers," Opt. Lett. **31**, 1797–1799 (2006).
25. V. Degiorgio, L. Tartara, R. Cherif, and M. Zghal, "Supercontinuum generation by higher-order mode excitation in a photonic crystal fiber," Eur. Conf. on Opt. Commun. Ecoc p. 5287128 (2009).